Available online at www.sciencedirect.com

ScienceDirect

Procedia Structural Integrity 17 (2019) 64–71

Structural Integrity Procedia

www.elsevier.com/locate/procedia

ICSI 2019 The 3rd International Conference on Structural Integrity

Numerical analysis of pitting corrosion fatigue in floating offshore wind turbine foundations

Behrooz Tafazzoli Moghaddam[a], Ali Mahboob Hamedany[a], Ali Mehmanparast[a], Feargal Brennan[b], Kamran Nikbin[c], Catrin Mair Davies[c]

[a] *Centre for Renewable Energy Technology, Cranfield University, Cranfield, MK43 0AL, UK.*
[b] *Department of Naval Architecture, Ocean and Marine Engineering, University of Strathclyde, Glasgow, G1 1XQ, UK.*
[c] *Department of Mechanical Engineering, Imperial College London, South Kensington Campus, London, SW7 2AZ, UK.*

Abstract

The mooring system of offshore floating wind foundations, which anchors the floating foundations to the seabed, sustains large dynamic loads during operation. The mooring chains are connected to the floating foundation below the water level through fairleads and chain-stoppers. The corrosive marine environment and the cyclic loading make the mooring connection prone to corrosion pitting and fatigue crack initiation and propagation from the pits, particularly in the weld zones. In this study, a finite element analysis of the crack growth from corrosion pits has been performed and the results are presented in order to provide an estimate of the extent of damage after the crack is detected. A Python script have been developed which generates the pit profiles based on a non-uniform random distribution of pit dimensions. 3D pits and elliptical cracks are embedded at critical points of weldment on the mooring point and analysed using ABAQUS XFEM. The Walker's model has been applied in the model to examine the effect of realistic R ratios in floating structures on pitting corrosion fatigue crack propagation along with direct cyclic solver. The numerical results obtained from this study are discussed in terms of the corrosion pitting effects on fatigue crack propagation behaviour in Spar-type floating offshore wind turbine foundations.

Peer-review under responsibility of the ICSI 2019 organizers.

Keywords: Corrosion fatigue, extreme value statistics, Rainflow cycle counting, floating offshore wind turbine, XFEM

* Ali Mehmanparast. Tel.: +44 (0) 1234 758331
Email address: a.mehmanparast@cranfield.ac.uk

2452-3216
Peer-review under responsibility of the ICSI 2019 organizers.
10.1016/j.prostr.2019.08.010

Nomenclature

A	Paris law coefficient
a	crack length
$f(z)$	density of probability
$f_e(z)$	density of probability
n	Paris law exponent
N	number of cycles
N_p	number of sampled pit depths
K	stress intensity factor
T	time
z_e	extreme value of the depth
μ_n	mean value for pit depth
μ_e	Location parameter for extreme value distribution
σ_e	scale parameter for pit distribution
WM	Weld Material
HAZ	Heat Affected Zone

1. Introduction

Offshore wind energy has experienced enormous expansion in the past decade and more development is planned amid climate change concerns. Based on WindEurope's analysis, 323 GW of wind energy capacity can be installed in the EU by 2030, of which 70 GW is offshore (EWEA, 2015). In the UK, 20-55 GW of offshore wind is expected by 2050 (James & Costa Ros, 2015). The dominant majority of installed offshore wind turbines are supported by fixed-bottom foundation structures in shallow waters. The near-shore waters are becoming scare and the industry is now moving toward floating foundations for deeper water, which poses great technical challenges to make it economically feasible.

The floating offshore wind turbine foundation is a key component in the structure's stability and it consumes a large proportion of the total cost of the structure. The floating foundations are fixed to the seabed by mooring lines. The foundation is continually subjected to large cyclic loads which causes fluctuating stresses with various amplitudes/frequencies. For a welded steel structure, this can increase the chance of corrosion pitting and fatigue crack initiation/growth from corrosion pits. Even if cathodic protection is used, corrosion pitting should not be neglected considering the life span of the structure (Melchers, 2010). Besides having a more complex structure, mooring points are the components that sustain all the structural loads caused by the movement of the structure and can be more susceptible to fatigue corrosion. In particular, the heat affected zone (HAZ) and weld metal (WM) regions of welded structures in marine environments are vulnerable locations for corrosion pitting (Chavez & Melchers, 2011). Corrosion fatigue fracture process can be divided into four stages (Larrosa, et al., 2017); surface film breakdown, pit growth, pit to crack transition, and cracking (short and long cracks). The first three stages comprise a significant portion of the structures life before fracture is started. Even in the cracking stage, the crack growth rate needs to exceed that of general corrosion before it can extend into a critical crack size. In the present study, the focus is on the fatigue behaviour of the long crack and the initiation and transition time to long crack is not considered. The analysis is focused on the points in which the long cracks are either predicted or spotted by NDT, and the aim is to offer a fracture mechanics based analysis to describe the crack growth and its effect on the structure's integrity.

The structural integrity of welded components mainly rely on stress-based approaches of unflawed structures (BS 7910, 2013). The stresses can be measured using finite element analysis (FE) of the intact structure in conjunction with appropriate stress concentration factors. Here, a fracture mechanics approach is applied while the cracks from pits are explicitly modelled on the structure. In this way, the actual flaw is integrated into the structure and fracture mechanics parameters are measured to characterise the crack growth behaviour. A numerical approach is proposed to simulate the crack growth from pits on critical spots on a mooring point for operational loads over several years to

find if the crack grows to critical state. The cracks are defined using ABAQUS XFEM and a direct cyclic solver simulates the crack growth over millions of cycles. The cyclic loads are identified from a load analysis that was carried out in a separate study using HydroDyn and FAST software (NERL, 2019). Rainflow cycle counting technique (Downing & Socie, 1982) is used to decompose the loads into simple cyclic loads for fatigue analysis.

2. Material degradation due to corrosion

2.1. Pit dimensions and general corrosion

Pitting corrosion of mild steel starts in early stages of exposure time to marine environment. Pits with radius of 100-200 microns initially appear (Melchers, 2004) and then become wider and deeper as time passes. The pitting is a very stochastic and time dependent process and new pits are continually created while the previously initiated ones grow. According to the experimental results in the literature (Aziz, 1956), most of the pits are generated in the initial stage of exposure and the rate of newly formed pits decays with time. In order to track the pitting process, statistical techniques such as extreme value statistics (Nicodemi, 2012) are used to predict the pit depth distribution over time. This technique also allows to predict the pit depth distribution when the measurement is done over a small area, which decrease the chance of missing largest possible pit. In addition, from the fracture mechanics point of view, the dominant large pits/cracks are of interest since the stress concentration and intensity factors are proportional to the dimensions of the pits. Fig.1 illustrates the pit dimension distribution and the extreme value definition over time. In this work, the pit profile is generated using extreme value distribution mathematics.

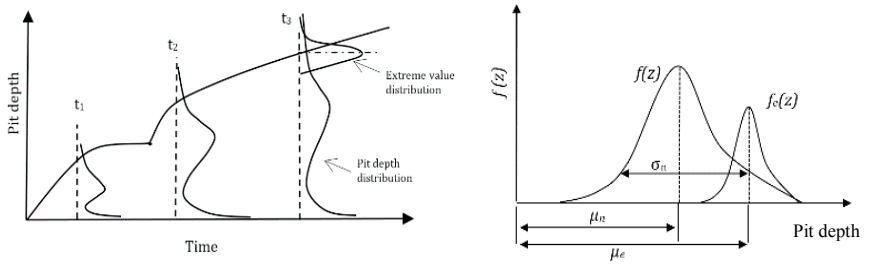

Figure 1 Pit depth distribution over time and extreme value distribution (Strutt, et al., 1985)

$$f_I(z_e) = exp(-exp(-\frac{(z_e-\mu e)}{\sigma_e})) \quad (1)$$

In Fig. 1 and Eqn. 1, $f(z)$ is the cumulative distribution function and z is the pit depth. e stands for extreme value and $f_I(z_e)$ is the extreme probability density function (Fig. 2). Now, μ_e (location parameter) and σ_e(scale parameter) can be calculated from μ_n and σ_n, which are mean pit depth value (for all pits) and standard deviation of the normal distribution respectively (Strutt, et al., 1985):

$$\mu_e = \mu_n + Y\sigma_n\,, \quad \sigma_e = S\mu_n \quad (2)$$

And

$$Y = \frac{2\,Ln\,N_p - 0.5Ln\,Ln\,N_p - Ln(2\sqrt{N_p})}{\sqrt{2LnN_p}} \quad and \quad S = \frac{1}{\sqrt{2Ln\,N_p}} \quad (3)$$

The experimental data for marine steel is scarce. For this study, the pit dimensions are taken from work of Chavez et al. (Chavez & Melchers, 2011) which is for three zones of welded specimen. They followed 5 deepest pits in each region over 3.5 years. This experiment was performed in Pacific Ocean in a half-tidal marine environment. Although the mooring points were submerged, using this data is conservative since the corrosion rate is higher in tidal regions (Momber, 2011). Fig. 2 shows an example of the generated density of probability for the 3.5 year time in HAZ using formula 1. Similar plots can be created for other times/regions as long as the average and extreme values for the target group of pits are given.

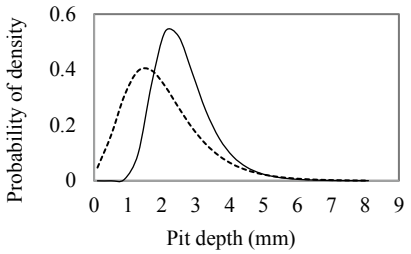

Figure 2 Probability of density for pit depths in HAZ at 3.5 years for all pits (dashed line) and the extreme value distribution (solid line)

A python script was developed to generate 3D pits on the mooring point based on the probability of density distributions for HAZ and WZ for the pit dimensions. Base material pits are not considered as the stress levels and pitting severity is much higher in HAZ and WZ.

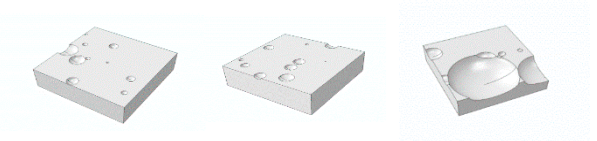

Figure 3 Example of randomly generated pits for different years at HAZ (1, 2 and 3.5 years)

2.2. General corrosion rates

In order for a crack to grow and cause failure, it has to surpass the general corrosion rate, otherwise the crack geometry will be exfoliated and no fatigue crack growth will occur. The general corrosion rate is highly dependent on the temperature and chemical composition of seawater. Melchers (Melchers, 2006) provided a temperature dependent distribution for corrosion loss and considering the North Sea average temperature to be around 8-10 °C, 0.2 mm/year corrosion was considered for the OC3 Hywind foundation. Also, (Momber, 2011) provided the underwater and splash zone corrosion rates for different offshore locations in the world and it suggests 0.14 mm/year for England (port facility).

3. Numerical Implementation

In this study, the structure of interest is 'OC3-Hywind' spar-buoy platform for 5MW NREL offshore baseline wind turbine (Bae, et al., 2011). The mooring lines are connected to the foundation in the arrangement depicted in Fig. 4. The mooring lines have 120 degrees angle between them and for the simulation, one mooring point is created in ABAQUS (Fig. 5). 30 mm S355 steel plates are considered for the mooring point. The mooring loads are transmitted onto the mooring points via cradles, which are pinned onto the mooring points. The pin load is simulated using equation constraint in ABAQUS such that it only sustain horizontal load on the vertical surfaces around the pins and the vertical load is put on the surface that cradle sits (Fig.5). The structure is partitioned such that high concentration of mesh is achieved around the pits and the mesh size gradually increases further away, to minimize the number of elements.

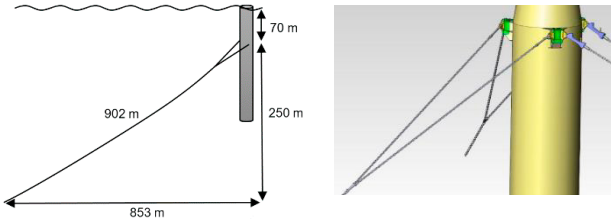

Figure 4 Mooring lines connected to the foundation in star shape. Image on the right from (Steen, 2016)

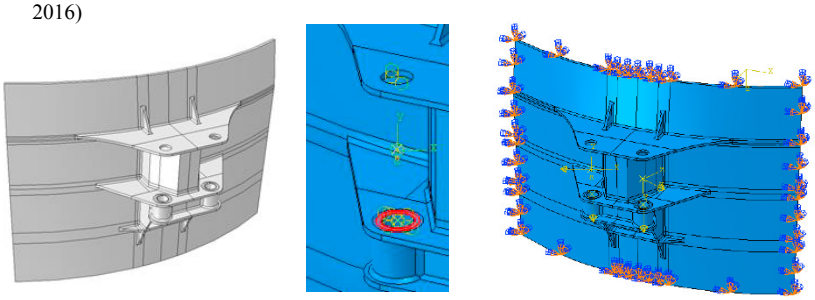

Figure 5 CAD drawing for the mooring point and foundation section and the boundary conditions.

3.1. Direct Cyclic solver and Paris law

ABAQUS direct cyclic solver is used for fatigue crack simulation. The cracks from pits are defined explicitly using extended finite element method (XFEM) on randomly generated 3D pits. When multiple cracks are present, separate cells should be defined for each crack individually. The crack planes are placed in the pit at an angle perpendicular to the direction of the maximum principal stress, which was calculated in an initial FE simulation without cracks (Fig. 6). Elements ranging from 0.3 to 1 mm were generated around the pits to fully capture the crack dimensions. The solver applies one cyclic load at a given step and finds a stabilized response of the structure iteratively. When the stabilized state is achieved, the energy release rates change between maximum and minimum load is measured to calculate the crack growth rate using Paris law (SIMULA, 2017).

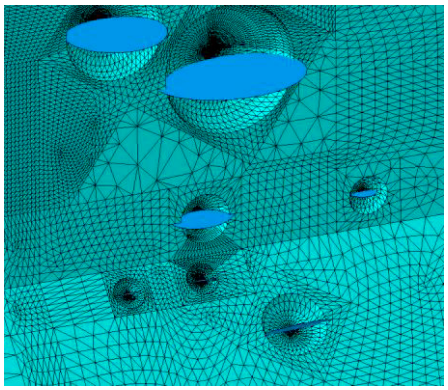

Figure 6 Example of XFEM cracks placed at randomly created pits on the mooring point critical spots

Paris law constants are taken from SLIC experimental results (Mehmanparast, et al., 2017) which is for R = 0.1. The cyclic stresses in floating offshore wind turbines have higher R values. Walker formula (Walker, 1970) is used in order to adjust the crack growth rate for different R values:

$$\frac{da}{dN} = A\left[\frac{\Delta K}{(1-R)^{(1-\gamma)}}\right]^n \quad (4)$$

As seen in Equation 4, γ controls the sensitivity to the changes in R ratio. For the current study $\gamma = 0.6$ is used (Dowling, 2004). The values for Paris law constants are reported in Table 2. These values are calculated using reference values at R = 0.1. The critical SIF is 542 MPa √m (Mehmanparast, et al., 2018). In this study only subcritical loading is considered in the Paris law region, for ΔK between 0 and 30% of K_{IC}.

Table 2. Paris law constants for different R ratios (for K in MPa √m)

R ratio	A	n
0.1	6.29e-12	3.23
0.5	1.34e-11	3.23

Only one value for Paris law is allowed for the direct cyclic solver in ABAQUS. For this reason, HAZ properties for the fatigue crack growth are used, as a conservative approach, since it has the highest growth rate compared to the WM and the base metal. Elastic modulus of S355 are used for all the zones as the difference is negligible. Several direct cyclic analysis steps can be used in the simulations which will allow application of different cyclic loads. Each cyclic load case defined from the result of Rainflow cycle counting is used in a separate step with its corresponding number of cycles.

3.2. Cyclic loads in mooring lines

Sample data for 11 wind speeds with 6 wave seeds in each category was used in the simulation. The loading data is broken down into simple load cycles using Rainflow cycle counting algorithm in order to carry out fatigue analysis. The identified cycles and the number of their repetition are calculated considering the probability of each wind speed occurrence. In total, 18 different subgroups were generated, comprising nearly 3 million cycles every year. These 18 cyclic load sets have four load components for the two bridles of each mooring point. The four components are applied in the arrangement illustrated in Fig. 5. The tests were executed for a 2 year time period and for R = 0.1 and 0.5.

4. Result

The results from quasi-static simulation of the flawless structure shows that the cyclic stresses have the highest magnitude near the weld fillet. Table 2 shows what range of mean values and amplitudes the cyclic stresses have. The cyclic loads in every category can have different frequency but in this study the effect of varying frequency on the crack grow is not considered.

Table 2. Cyclic stresses near weldment and their frequency

Amplitude (MPa)	Mean stress (MPa)	Cycle/hour
2-8	60-90	309
12-39	75-100	19

The stress distribution around the pits/cracks and the crack growth are illustrated in Fig. 7. The crack growth rate is plotted for different R ratios and at different zones (Fig. 8). Higher R ratios clearly experience larger crack growth rates. In HAZ, maximum 0.69 mm/year growth occurred for R = 0.5 at pit 5.

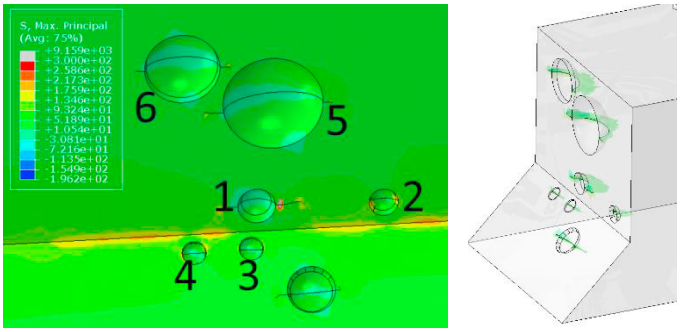

Figure 7 Crack growth from pits at HAZ and WM

Table 3 summarizes the growth for all the pits in one year. The cracks that exceeded the general corrosino rate are shown in bold text. Pits 5 & 6 show high crack growth rate above the general corrosion, dispite having lower stresses since they are not close to the weld. These two pits have large initial dimensions, resulting in higher stress intensity factor and subsequently larger crack growth . The results suggest that the factors that decide whether the crack can survive the general corrosion are the size of the pit and the location of the crack.

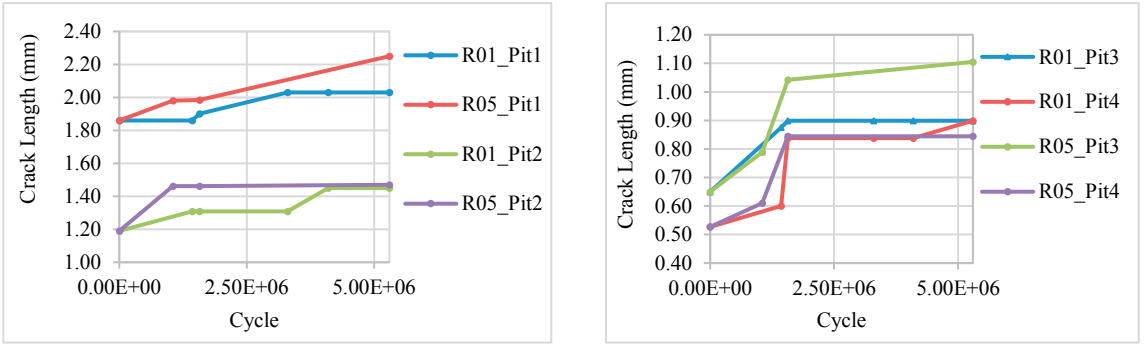

Figure 8 Crack grow for two years in HAZ (left) and WM for different R ratios

The outcome highlights the importance of R ratio effect on corrosion fatigue crack growth analysis of offshore wind turbine floating foundations. The cyclic stresses in the mooring point have high R ratios and accurate Paris law constants are essential to be employed in the analysis. It should be noted that using Walker's formula for Paris constant manipulation might overestimate the crack growth rates and the dependency of the changes to R ratio can varry for different structural steels. For instance, de Jesus, et al. argues that the crack growth rate increase happens when R changes from 0 to a positive value and after that, increase in R does not change the crack grow rate significantly (de Jesus, et al., 2012).

Table 3. Pit depth growth (mm) in one year for pits in Fig. 8.

Pit #	1	2	3	4	5	6
a0 (mm)	1.86	1.19	0.65	0.52	2.4	1.88
R=0.1	0.069	0.13	0.12	0.18	0.22	**0.21**
R=0.5	0.19	0.14	**0.20**	0.15	**0.69**	**0.22**

5. Conclusion

Aframework bass been defined for the analysis of fatigue cracks from corrosion pits on the mooring point of floating wind foundations. The pits were created randomly on the critical spots at the weldment using extreme value

distributino for the pit depths, based on available experimental data for steel in marine environment. The cracks from pits were simulated using ABAQUS XFEM in conjunction with direct cyclic solver.

Another acheivment of the study is the definition of cyclic loads from a dynamic analysis results for mooring line forces. Nearly 40,000 seconds of loading data on three mooring lines where analysed and the cyclic loads were identified and grouped into 18 subgroups, which were applied one by one in direct cyclic steps.

The crack growth simulation was carried out for multiple cracks over a two year time to see whether they surpasses the general corrosion rates. The results indicate that the initial size of the pit/crack is the most important factor in crack growth rate and at high R ratios, which is common in floating foundations, the crack grow rate can exceed the general corrosion rate for the initial cracks larger than 1.8 mm, although exceptions exist depending on the pit location. HAZ material experiences more damage since the pitting is more severe and larger depths are more probable. The study highlights the fact that larger R ratios will result in higher crack growth rates, as calculated by Walker formula. This also emphasizes the importance of having accurate experimental test results for these specific R ratios as well as the effect of frequency on the corrosion fatigue crack growth rate.

References

Aziz, P. M., 1956. Application of the statistical theory of extreme values to the analysis of maximum pit depth data for aluminum. *Corrosion,* 12(10), pp. 35-46.

Bae, Y. H., Kim, M. H., Im, S. W. & Chang, I. H., 2011. *Aero-elastic-control-floater-mooring coupled dynamic analysis of floating offshore wind turbines.* Maui, Hawaii, s.n.

BS 7910, 2013. *Guide on methods for assessing the acceptability,* s.l.: London: British Standard Institution.

Chavez, I. A. & Melchers, R. E., 2011. Pitting corrosion in pipeline steel weld zones. *Corrosion Science,* 53(12), pp. 4026-4032.

de Jesus, A. M. et al., 2012. A comparison of the fatigue behavior between S355 and S690 steel grades. *Journal of Constructional Steel Research,* Volume 79, pp. 140-150.

Dowling, N. E., 2004. Mean stress effects in stress-life and strain-life fatigue. *SAE Technical Paper (2004-01-2227).*

Downing , S. D. & Socie, D. F., 1982. Simple Rainflow Counting Algorithms. *International journal of fatigue,* 4(1), pp. 31-40.

EWEA, 2015. *Wind energy in Europe, Scenarios for 2030, Bruccels, Belgium.* [Online]
Available at: https://windeurope.org/about-wind/reports/wind-energy-in-europe-scenarios-for-2030/, [Accessed 2019].

James, R. & Costa Ros, M., 2015. *Floating Offshore Wind:Market and Technology Review,* s.l.: CARBON TRUST.

Larrosa, N. O., Akid, R. & Ainsworth, R. A., 2017. Corrosion-fatigue: a review of damage tolerance models. *nternational Materials Reviews,* 63(5), pp. 283-308.

Mehmanparast, A., Brennan, F. & Tavares, I., 2017. Fatigue crack growth rates for offshore wind monopile weldments in air and seawater: SLIC inter-laboratory test results. *Materials & Design,* Volume 114, pp. 494-504.

Mehmanparast, A., Taylor, J., Brennan, F. & Tavares, I., 2018. Experimental investigation of mechanical and fracture properties of offshore wind monopile weldments: SLIC interlaboratory test results. *Fatigue & Fracture of Engineering Materials & Structures,* 41(12), pp. 2485-2501.

Melchers, R., 2004. Pitting Corrosion of mild steel in marine immersion environment - Part 1: Maximum pit depth. *Corrosion,* 9(8), pp. 824-836.

Melchers, R., 2010. The changing character of long term marine corrosion of mild steel.

Melchers, R. E., 2006. Recent Progress in the Modeling of Corrosion of Structural steel immersed in seawater. *Journal of infrastructure systems,* 12(3), pp. 154-162.

Momber, A., 2011. Corrosion and corrosion protection of support structures for offshore wind energy devices (OWEA). *Materials and Corrosion,* 62(5), pp. 391-404.

NERL, 2019. *NWTC Information Portal: Software.* [Online], Available at: https://nwtc.nrel.gov/Software, [Accessed 2019].

Nicodemi, M., 2012. *Extreme Value Statistics: Theory, Techniques, and Applications.* New York: Springer New York.

SIMULA, 2017. *ABAQUS Documentation.* [Online]
Available at: https://www.sharcnet.ca/Software/Abaqus/6.14.2/v6.14/books/usb/default.htm?startat=pt01ch03s02abx11.html [Accessed 2019].

Steen, K. E., 2016. *Hywind Scotland – status and plans.* [Online]
Available at: https://www.sintef.no/globalassets/project/eera-deepwind2016/presentations/steen_opening-session.pdf, [Accessed 2019].

Strutt, J. E., Nicholls, J. R. & Barbier, B., 1985. The prediction of corrosion by statistical analysis of corrosion profiles. *Corrosion Science,* 25(5), pp. 305-315.

Walker, K., 1970. The effect of stress ratio during crack propagation and fatigue for 2024-T3 and 7075-T6 aluminum, in Effects of Environment and Complex Load History on Fatigue Life, ASTM STP 462. *American Society for Testing and Materials,* pp. 1-14.